

# Self-healing materials with microvascular networks

KATHLEEN S. TOOHEY<sup>1,2</sup>, NANCY R. SOTTOS<sup>2,3\*</sup>, JENNIFER A. LEWIS<sup>2,3</sup>, JEFFREY S. MOORE<sup>2,4</sup>  
AND SCOTT R. WHITE<sup>2,5</sup>

<sup>1</sup>Department of Mechanical Science and Engineering, University of Illinois at Urbana-Champaign, Urbana, Illinois 61801, USA

<sup>2</sup>Beckman Institute, University of Illinois at Urbana-Champaign, Urbana, Illinois 61801, USA

<sup>3</sup>Department of Materials Science and Engineering, University of Illinois at Urbana-Champaign, Urbana, Illinois 61801, USA

<sup>4</sup>Department of Chemistry, University of Illinois at Urbana-Champaign, Urbana, Illinois 61801, USA

<sup>5</sup>Department of Aerospace Engineering, University of Illinois at Urbana-Champaign, Urbana, Illinois 61801, USA

\*e-mail: n-sottos@uiuc.edu

Published online: 10 June 2007; doi:10.1038/nmat1934

**Self-healing polymers composed of microencapsulated healing agents exhibit remarkable mechanical performance and regenerative ability<sup>1–3</sup>, but are limited to autonomic repair of a single damage event in a given location. Self-healing is triggered by crack-induced rupture of the embedded capsules; thus, once a localized region is depleted of healing agent, further repair is precluded. Re-mendable polymers<sup>4,5</sup> can achieve multiple healing cycles, but require external intervention in the form of heat treatment and applied pressure. Here, we report a self-healing system capable of autonomously repairing repeated damage events. Our bio-inspired coating–substrate design delivers healing agent to cracks in a polymer coating via a three-dimensional microvascular network<sup>6</sup> embedded in the substrate. Crack damage in the epoxy coating is healed repeatedly. This approach opens new avenues for continuous delivery of healing agents for self-repair as well as other active species for additional functionality.**

Healing in biological systems is accomplished by a pervasive vascular network that supplies the necessary biochemical components. Recent advances in soft lithographic and direct-write assembly methods have enabled the creation of materials with complex embedded microvascular networks that emulate many of the key responses of biological vascular systems<sup>6–9</sup>. To demonstrate the use of microvascular networks for autonomic healing of structural damage, we explore a microvascular coating–substrate architecture that mimics human skin (Fig. 1a). The outer epidermal layer of skin is composed of multiple sublayers that work in concert to continually rebuild the surface of the skin, whereas the underlying dermal layer supplies the epidermis with nutrient-laden blood and regulates temperature. Because skin serves as a protective barrier, any damage must be rapidly and efficiently healed<sup>10</sup>. A cut in the skin triggers blood flow from the capillary network in the dermal layer to the wound site rapidly forming a clot that serves as a matrix through which cells and growth factors migrate as healing ensues. Owing to the vascular nature of this supply system, minor damage to the same area can be healed repeatedly.

Our self-healing microvascular coating–substrate design is shown in Fig. 1b. An epoxy coating is deposited on a more ductile substrate that contains a pervasive three-dimensional (3D) microvascular network. Solid catalyst particles are incorporated

within the coating and the network is filled with a liquid healing agent. The coating–substrate beam is loaded in four-point bending until crack initiation occurs at the surface of the coating, where the tensile stress is maximum. The resulting cracks are attracted to the more compliant regions of the substrate created by the presence of fluid-filled microchannels and then arrested at the coating–substrate interface (Fig. 1c). After damage occurs in the coating, healing agent wicks from the microchannels into the crack(s) through capillary action. No external pressure is required. Similar damage-triggered release mechanisms have been explored in self-sealing tyres with a viscous gel layer<sup>11</sup> and surgical gloves with sequestered droplets of biocide<sup>12</sup>. The efficiency of this release and delivery mechanism is shown in Fig. 1d, in which excess healing agent is present on the surface of the coating after initial crack formation. Once in the crack plane, the healing agent interacts with the catalyst particles in the coating to initiate polymerization, rebonding the crack faces autonomically. After a sufficient time period, the cracks are healed and the structural integrity of the coating is restored. As cracks reopen under subsequent loading, the healing cycle is repeated.

The self-healing process requires a suitable chemistry to polymerize the healing agent in the fracture plane. Although the microvascular approach opens up a broad range of potential chemistries, healing of the coating is first demonstrated via ring-opening metathesis polymerization of dicyclopentadiene (DCPD) monomer by Grubbs' catalyst, benzylidene-bis(tricyclohexylphosphine) dichlororuthenium, which was used successfully in previous microencapsulated composites<sup>1–3,13–16</sup>. This materials system satisfies several requirements critical for achieving high healing efficiency in this new architecture. First, the healing agent possesses a low viscosity, which facilitates its flow into the crack plane and allows for complete coverage of the exposed surfaces. Second, this solid-phase catalyst remains reactive during and after curing of the coating. Finally, the catalyst particles quickly dissolve on contact with the monomer in the crack plane and polymerize the DCPD under ambient conditions, producing a tough crosslinked polymer (see the Supplementary Information).

To create the architecture in Fig. 1b, we embed a 3D microvascular network in the polymer substrate via direct-write assembly of a fugitive organic ink<sup>6,17</sup>. A rectangular network

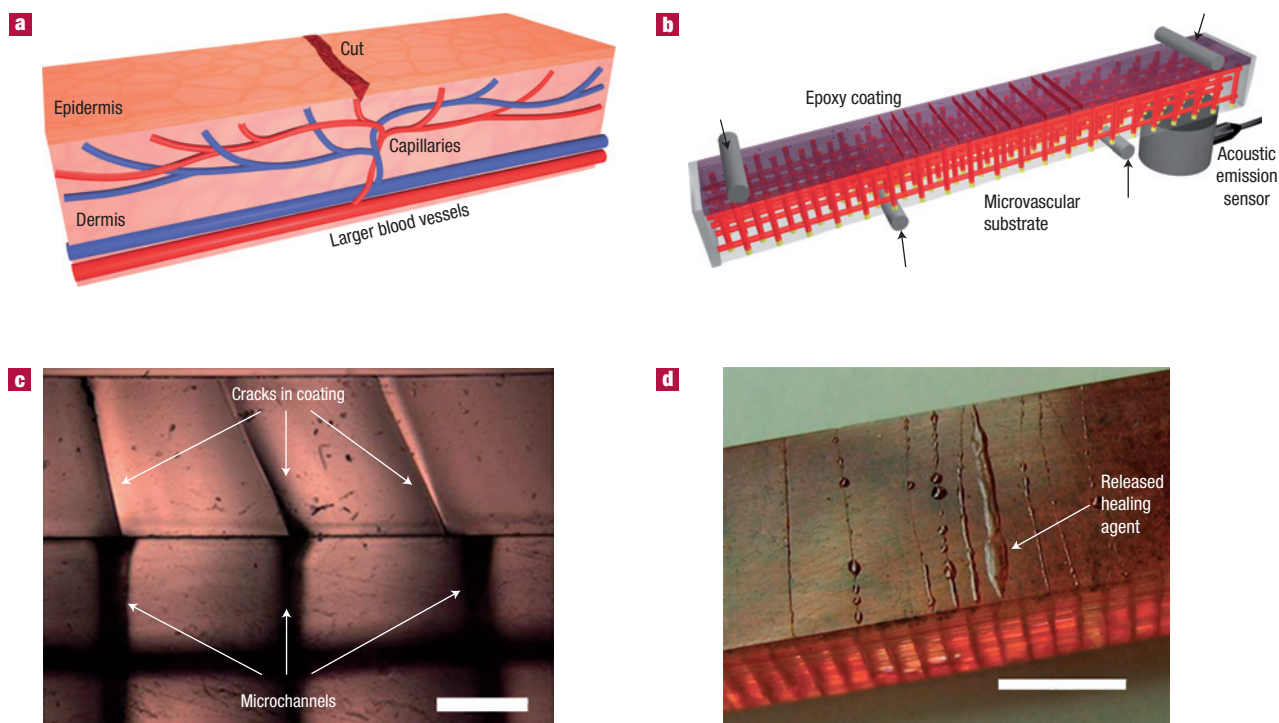


**Figure 1** Self-healing materials with 3D microvascular networks. **a**, Schematic diagram of a capillary network in the dermis layer of skin with a cut in the epidermis layer. **b**, Schematic diagram of the self-healing structure composed of a microvascular substrate and a brittle epoxy coating containing embedded catalyst in a four-point bending configuration monitored with an acoustic-emission sensor. **c**, High-magnification cross-sectional image of the coating showing that cracks, which initiate at the surface, propagate towards the microchannel openings at the interface (scale bar = 0.5 mm). **d**, Optical image of self-healing structure after cracks are formed in the coating (with 2.5 wt% catalyst), revealing the presence of excess healing fluid on the coating surface (scale bar = 5 mm).

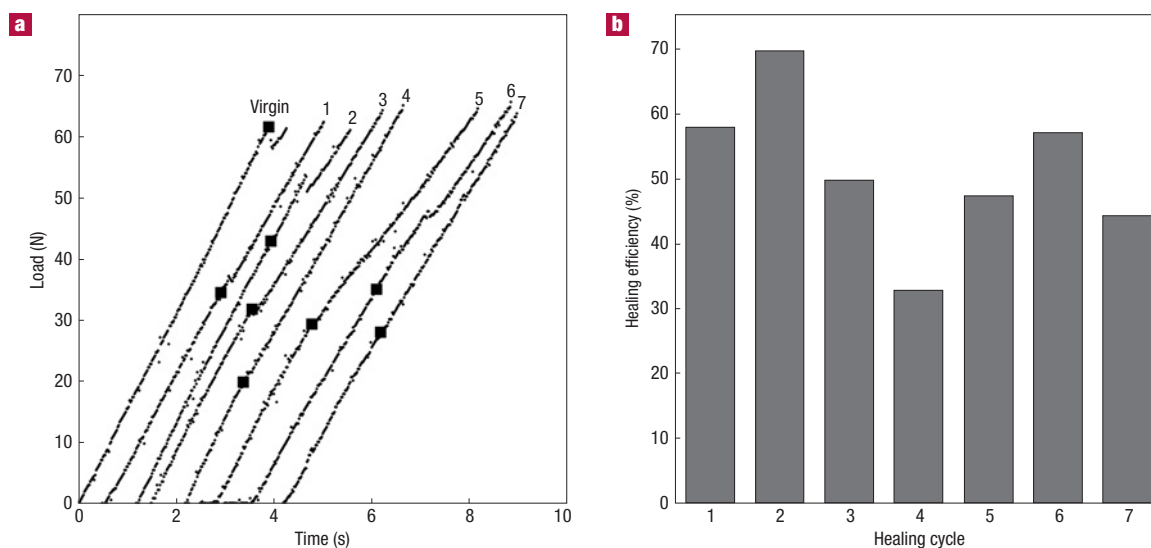


**Figure 2** Mechanical behaviour and healing efficiency. **a**, Load data for the virgin- and healed-specimen tests (1–7) for the best specimen, where the large squares denote the critical crack event for each. Loading traces were shifted 200–500 ms to visualize each data set individually. **b**, Healing efficiency for each successive loading of this coated microvascular beam (10 wt% catalyst in the coating).

design is chosen for this initial healing demonstration in which the vertical channels deliver monomer to the cracks in the coating, whereas the horizontal channels enable the network to

be filled from the side. 3D periodic scaffolds are fabricated by depositing the ink in a layer-by-layer build sequence followed by infiltration with an epoxy resin. The resin is then cured and

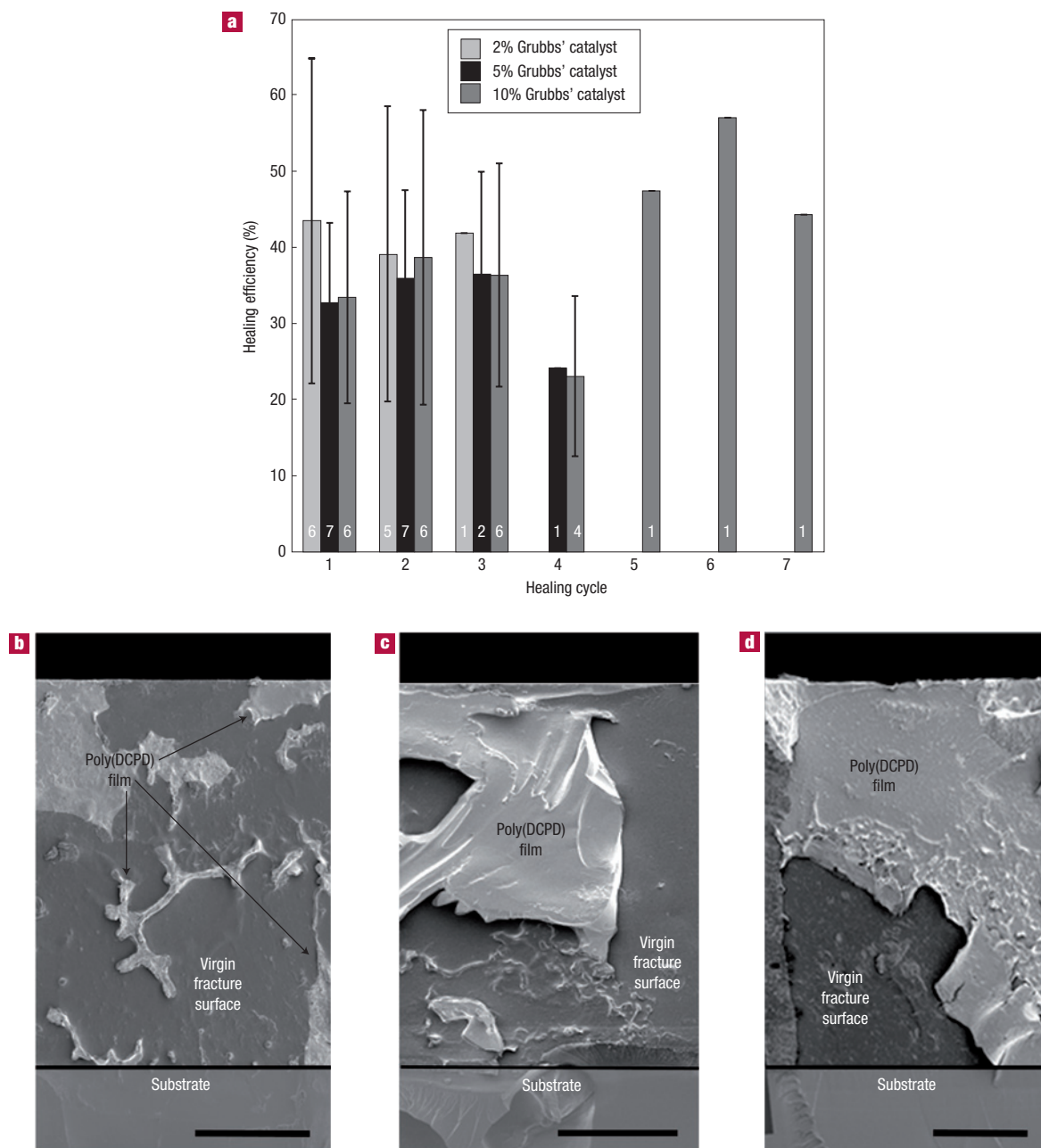


**Figure 3** Grubbs' catalyst effects on healing efficiency. **a**, Average healing efficiency for specimens with 2 wt%, 5 wt% and 10 wt% catalyst in the coating that exhibited healing. The white numbers at the bottom of each column denote the number of successfully healed specimens in the average and the error bars are one standard deviation. **b–d**, Scanning electron micrographs of the fracture plane after one healing cycle for a coating with 5 wt% catalyst (**b**), after four healing cycles with 5 wt% catalyst (**c**) and after seven healing cycles with 10 wt% catalyst (**d**) (scale bars = 200  $\mu\text{m}$ ).

the fugitive ink is subsequently removed under a light vacuum by heating the structure to modest temperatures to liquefy the ink. As the presence of channels impacts the structural properties of the substrate, networks with maximum channel spacing and minimum channel diameter are desirable. The spacing between channels in a given layer is limited to approximately ten times the channel diameter owing to the viscoelastic properties of the fugitive ink<sup>6</sup>. In addition, the channel diameter must be large enough for healing agent to flow through the network to the cracks in the coating. The chosen channel diameter of 200  $\mu\text{m}$

is sufficiently small to minimize the total pore volume, yet large enough for ease of fabrication and network operation. A more brittle epoxy coating (approximately 700  $\mu\text{m}$  thick) containing Grubbs' catalyst particles is applied to the top surface of the microvascular substrate, as shown in Fig. 1b. Concentrations of 0% (control), 2%, 5% and 10% by weight of catalyst are added to the epoxy coating to investigate the effect of catalyst concentration on healing performance.

Autonomic healing efficiency is evaluated on the basis of the ability of the healed coating to recover fracture toughness. The

coated microvascular substrates are filled with DCPD healing agent and then sealed (see the Supplementary Information). The coating–substrate beams are loaded in four-point bending to initiate a single crack in the coating without damaging the underlying microvascular substrate. With each loading cycle, the same crack reopens and is subsequently healed repeatedly. An acoustic-emission sensor is placed on the beam to detect the crack-opening events during testing. The time at which the critical acoustic-emission event occurs is used to determine the loads of crack formation and reopening in the virgin- and healed-specimen tests. Although Fig. 1c shows multiple cracks developed in the coating, quantitative healing tests are limited to a single crack by stopping the loading process after the first acoustic-emission signal is detected. In a small number of tests, new cracks did initiate in the coating during reloading. Specimens in which additional cracks formed are not subject to further testing to enable more accurate comparisons between different healing cycles and specimens. After testing, the coating is healed at room temperature (approximately 25 °C) for 12 h. Any excess DCPD monomer is removed from the network by applying a light vacuum. The network is then replenished with monomer before carrying out the next bend test. This cycle is repeated until the crack no longer heals. As described in the Methods section, healing efficiency is calculated for each healing cycle on the basis of the ratio of the critical loads for crack opening,  $\eta = P^{\text{Healed}}/P^{\text{Virgin}}$ .

The coated microvascular beams with high catalyst concentration (10 wt%) exhibit healing over the largest number of loading cycles. The critical forces on reopening of the original crack in each cycle, as detected by the acoustic-emission sensor, are denoted on the loading curves (Fig. 2a). The associated healing efficiency calculated for a series of seven consecutive healing cycles for the same crack is shown in Fig. 2b. Some scatter in the data occurs from one cycle to the next and the peak recovery (70%) is achieved after the second healing cycle. Beyond the seventh loading cycle, this specimen no longer healed.

The effect of Grubbs' catalyst concentration on healing performance is summarized in Fig. 3a. The concentration of catalyst in the coating did not significantly influence the average healing efficiency achieved by specimens for a given cycle. However, the amount of catalyst had a pronounced impact on the number of successful consecutive healing cycles achieved. Specimens containing 2 wt% catalyst healed a maximum of three times, whereas specimens with 5 wt% catalyst healed no more than four times, compared with a maximum of seven cycles for the highest catalyst concentration (10 wt%). The average number of successful healing events for each set was two, three and four cycles for specimens with 2 wt%, 5 wt% and 10 wt% catalyst, respectively, owing to fewer specimens continuing to heal after further testing (see the Supplementary Information). We note that control specimens with 0 wt% catalyst (not shown) did not heal. Because the Grubbs' catalyst undergoes some deactivation on exposure to amines in the uncured epoxy coating material<sup>18</sup>, the effective concentration of active catalyst is lower than the values stated.

Factors such as the reactivity, concentration and availability of Grubbs' catalyst affect both the kinetics and degree of polymerization of the healing agent in the crack plane. Scanning electron micrographs of these specimens reveal distinct differences in the coverage of polymerized DCPD on the crack surfaces. Typically, the fracture planes of coated microvascular beams with 2 wt% or 5 wt% catalyst contain small scattered patches of poly(DCPD) film (Fig. 3b) with localized regions of good coverage located near larger catalyst particles (approximately 500 µm). The poor coverage of poly(DCPD) on the crack surface is also associated with a low number of successful healing cycles. More

polymerized material covers the crack plane in coatings with the same catalyst concentration that exhibit healing over a larger number of cycles (Fig. 3c). In specimens with the highest catalyst concentration of 10 wt%, there is nearly complete coverage of the fracture plane with poly(DCPD) film in specimens (Fig. 3d). The large amount of healed material in the crack plane indicates a build-up of polymerized DCPD with each additional cycle of healing (see the Supplementary Information). Ultimately, the ability to achieve further healing events in these specimens is controlled by the availability of active catalyst in the coating. With each cycle of healing, less active catalyst is available and eventually the healing efficiency is degraded when no more active catalyst is accessible, even though there is a continuous supply of monomer.

The limitations associated with depletion of embedded catalyst and the need to resupply multiple healing agents within these architectures may be overcome by implementing a new microvascular design based on interdigitated dual networks. This improved design will allow new healing chemistries (for example, two-part epoxies<sup>19</sup>) to be exploited, which could ultimately lead to unlimited healing capability. We imagine extending this approach further to integrate pumps, valves and internal reservoirs, as well as to introduce new functionalities, including self-diagnosis or self-cooling, through the circulation of molecular signals, coolants or other species.

## METHODS

### MICROVASCULAR SUBSTRATE FABRICATION

Direct-write assembly<sup>6,17</sup> is used to embed fully interconnected 3D microchannel network(s) in an epoxy matrix. 3D scaffolds are fabricated with a fugitive organic ink using a robotic deposition apparatus (Model JL2000, Robocasting Enterprises) in a layerwise scheme. The fugitive ink is composed of 60 wt% petroleum jelly (Vaseline, Chesebrough-Ponds) and 40 wt% microcrystalline wax (Bard's Tacky Wax, Bard) and housed in a syringe (barrel diameter = 9.5 mm) with a 200 µm cylindrical nozzle. This syringe is mounted on the z stage, which is suspended above a moving x–y stage. The three-axis motion is controlled during deposition using custom-designed software (Robocad version 2.0). The syringe is placed in a device (HP7X, EFD) that enhances the air pressure to approximately 2.9 MPa. 3D periodic scaffolds (45 mm × 7 mm × 10 mm) are fabricated, which are composed of an array of 200 µm cylindrical rods with a centre-to-centre separation distance of 2 mm between each rod in a given layer. Consecutive layers are rotated by 90° and every other layer is shifted by 1 mm in plane to create a face-centred tetragonal geometry. After deposition, the ink scaffold is infiltrated with uncured EnviroTex Lite epoxy (ETI) and allowed to cure at room temperature for 48 h. After curing, beam substrates are cut to size and polished. The fugitive ink is then removed by heating the substrate to 75 °C and applying a light vacuum. The bottom and sides of the substrate are sealed by selectively polymerizing a photopolymer (NOA 61, Norland Optical Adhesives) in the channels using a mercury source ( $\lambda = 365$  nm).

### CATALYST RECRYSTALLIZATION

The as-received Grubbs' catalyst<sup>20</sup>, benzylidene-bis(tricyclohexylphosphine) dichlororuthenium (Sigma-Aldrich), requires further processing to achieve better solubility in the DCPD. The catalyst is recrystallized using methylene chloride and acetone in a method described by Jones *et al.*<sup>16</sup>. The resulting catalyst crystals are composed of a rod-like morphology with an average length of 10 µm and diameter of 0.75 µm, which form larger aggregates with an average diameter of 150 µm.

### COATING APPLICATION

A brittle epoxy coating is produced by degassing 12 p.p.h. of diethylenetriamine (Air Products) in EPON 828 resin (Miller Stephenson) with the appropriate concentration of catalyst particles. On mixing the catalyst particles into the uncured epoxy, larger aggregates form. The mixture is poured into a mould, in which the microvascular substrate serves as the underlying substrate. The largest catalyst particles are excluded from the final coatings, but aggregates up

to 500  $\mu\text{m}$  in diameter remain. Before applying the coating, the microvascular substrate is filled with a fugitive wax (Purester 24, Strahl & Pitsch) to prevent the epoxy from infiltrating the microchannels. After curing for 24 h at room temperature, the coating is polished using lapping oil to the desired thickness (approximately 700  $\mu\text{m}$ ). A range of film thicknesses are explored (300–1,000  $\mu\text{m}$ ), and no significant affect on healing capability is found. The wax is then removed by heating the specimen to 35 °C for 8–10 min and applying a light vacuum. The specimens are allowed to post cure at 25 °C for 24 h before testing.

#### FRACTURE TEST

The coated microvascular beams are loaded in four-point bending to place the coating under tension. The lower span of the test fixture is 40 mm, the upper span is 20 mm and the crosshead speed is 50  $\mu\text{m s}^{-1}$ . Load–time data are collected using LabVIEW (version 6.5, National Instruments) software. An acoustic-emission sensor (model SE2MEG-P, Dunegan Engineering Company) is used to detect the occurrence of crack events during the healed-specimen tests. Data from the acoustic-emission sensor are collected with a digital oscilloscope (model LC584A, LeCroy) and then exported to a computer for correlation with the load–time data to determine the load at which the first crack reopened. A few specimens from each set are not included in the averaging owing to inconclusive acoustic-emission signals or additional cracking of the coating.

#### FRACTURE TOUGHNESS ANALYSIS

In a series of papers by Nairn and Kim<sup>21–23</sup>, a finite fracture-mechanics model is developed to predict the formation of cracks in a thin coating on a substrate loaded in four-point bending. The strain energy for a single crack interval is found and then differentiated to find the mechanical energy release rate. The total energy release rate is a combination of the energy due to mechanical loading and residual stresses in the coating<sup>22</sup>. The fracture toughness for the formation for the first crack in four-point bending is found to be

$$K_{Ic} = \sqrt{EC_3 t \left( \frac{P(a-b)y}{4I} \right)^2 \lim_{D \rightarrow 0} Y(D)},$$

where  $E$  is the elastic modulus of the coating,  $t$  is the coating thickness,  $P$  is the applied load when the crack occurs,  $a$  and  $b$  are the outer- and inner-support spacing,  $y$  is the distance from the neutral axis to the top surface of the coating and  $I$  is the moment of inertia of the composite beam. The variables  $C_3$  and the limit of  $Y(D)$  as crack density ( $D$ ) approaches zero are functions of the geometry of the beam and are found through a variational mechanics analysis<sup>21,23</sup>. Here, the residual stress is neglected, as the coating is cured at room temperature. The healing efficiency for a crack is

$$\eta = \frac{K_{Ic}^{\text{Healed}}}{K_{Ic}^{\text{Virgin}}}.$$

In a single specimen, the material properties and geometry do not change and the healing efficiency simplifies to a ratio of the healed and virgin loads,

$$\eta = \frac{P^{\text{Healed}}}{P^{\text{Virgin}}}.$$

Received 26 January 2007; accepted 11 May 2007; published 10 June 2007.

#### References

- White, S. R. *et al.* Autonomic healing of polymer composites. *Nature* **409**, 794–797 (2001).
- Brown, E. N., Sottos, N. R. & White, S. R. Fracture testing of a self healing polymer composite. *Exp. Mech.* **42**, 372–379 (2002).
- Brown, E. N., White, S. R. & Sottos, N. R. Retardation and repair of fatigue cracks in a microcapsule toughened epoxy composite—part II: In situ self-healing. *Compos. Sci. Technol.* **65**, 2474–2480 (2005).
- Chen, X. *et al.* A thermally re-mendable cross-linked polymeric material. *Science* **295**, 1698–1702 (2002).
- Chen, X., Wudl, F., Mal, A. K., Shen, H. & Nutt, S. R. New thermally remendable highly cross-linked polymeric materials. *Macromolecules* **36**, 1802–1807 (2003).
- Therriault, D., White, S. R. & Lewis, J. A. Chaotic mixing in three-dimensional microvascular networks fabricated by direct-write assembly. *Nature Mater.* **2**, 265–271 (2003).
- Runyon, M. K., Johnson-Kerner, B. L. & Ismagilov, R. F. Minimal functional models of hemostasis in a biomimetic microfluidic system. *Angew. Chem. Int. Edn* **43**, 1531–1536 (2004).
- Stroock, A. D. & Cabodi, M. Microfluidic biomaterials. *Mater. Res. Soc. Bull.* **31**, 114–119 (2006).
- Lim, D., Kamotani, Y., Cho, B., Mazumder, J. & Takayama, S. Fabrication of microfluidic mixers and artificial vasculatures using a high-brightness diode-pumped Nd:YAG laser direct write method. *Lab Chip* **3**, 318–323 (2003).
- Martin, P. Wound healing—Aiming for perfect skin regeneration. *Science* **276**, 75–81 (1997).
- Nagaya, K., Imai, S., Chiba, M. & Chao, X. Tire with self-repairing mechanism. *JSME Int. J.* **49**, 379–384 (2006).
- Sonntag, P. *et al.* Biocide squirting from an elastomeric tri-layer film. *Nature Mater.* **3**, 311–315 (2004).
- Kessler, M. R., Sottos, N. R. & White, S. R. Self-healing structural composite materials. *Compos. Part. A* **34**, 743–753 (2003).
- Brown, E. N., White, S. R. & Sottos, N. R. Microcapsule induced toughening in a self-healing polymer composite. *J. Mater. Sci.* **39**, 1703–1710 (2004).
- Brown, E. N., White, S. R. & Sottos, N. R. Retardation and repair of fatigue cracks in a microcapsule toughened epoxy composite—part I: Manual infiltration. *Compos. Sci. Technol.* **65**, 2466–2473 (2005).
- Jones, A. S., Rule, J. D., Moore, J. S., White, S. R. & Sottos, N. R. Catalyst morphology and dissolution kinetics for self-healing polymers. *Chem. Mater.* **18**, 1312–1317 (2005).
- Therriault, D. *Directed Assembly of Three-Dimensional Microvascular Networks*. Thesis, Univ. of Illinois at Urbana-Champaign (2003).
- Rule, J., Brown, E. N., Sottos, N. R., White, S. R. & Moore, J. S. Wax-protected catalyst microspheres for efficient self-healing materials. *Adv. Mater.* **72**, 205–208 (2005).
- Bond, I. & Pang, J. 'Bleeding composites'—enhanced damage detection and self repair using a biomimetic approach. *Compos. Part. A* **36**, 183–188 (2005).
- Schwab, P., Grubbs, R. H. & Ziller, J. W. Synthesis and applications of  $\text{RuCl}_2(=\text{CHR})(\text{PR}_3)_2$ : The influence of the alkylidene moiety on metathesis activity. *J. Am. Chem. Soc.* **118**, 100–110 (1996).
- Kim, S.-R. & Nairn, J. A. Fracture mechanics analysis of coating/substrate systems part I: Analysis of tensile and bending experiments. *Eng. Fract. Mech.* **65**, 573–593 (2000).
- Kim, S.-R. & Nairn, J. A. Fracture mechanics analysis of coating/substrate systems part II: Experiments in bending. *Eng. Fract. Mech.* **65**, 595–607 (2000).
- Nairn, J. A. & Kim, S.-R. A fracture mechanics analysis of multiple cracking in coatings. *Eng. Fract. Mech.* **42**, 195–208 (1992).

#### Acknowledgements

This work has been financially supported by the Air Force Office of Scientific Research Multidisciplinary University Research Initiative (grant number F49550-05-1-0346). K.S.T. is supported in part by the Beckman Institute for Advanced Science and Technology Graduate Fellows Program. We extend our gratitude to the Imaging Technology Group at the Beckman Institute, especially S. Robinson, for assistance with scanning electron microscopy. Correspondence and requests for materials should be addressed to N.R.S. Supplementary Information accompanies this paper on [www.nature.com/naturematerials](http://www.nature.com/naturematerials).

#### Author contributions

K.S.T. carried out all of the experiments and analysis. N.R.S. and S.R.W. conceived the microvascular substrate–coating experiment and directed the research. J.A.L. and S.R.W. developed the direct-write manufacturing method. J.S.M. assisted with the healing chemistry. All authors participated in discussions of the research and wrote the manuscript.

#### Competing financial interests

The authors declare no competing financial interests.

Reprints and permission information is available online at <http://npg.nature.com/reprintsandpermissions/>